International Journal of Science and Research Archive
eISSN: 2582-8185
Cross Ref DOI: 10.30574/ijsra
Journal homepage: https://ijsra.net/

(RESEARCH ARTICLE)

Check for updates

# DESIGN, STRUCTURAL ELUCIDATION, AND TARGETED CYTOTOXIC EVALUATION OF NOVEL METAL–SCHIFF BASE COMPLEXES AS POTENTIAL ANTICANCER AGENTS

Rehab M. Mustafa [1], Mostafa F. Mohamed [1], Abdou S. Eltabl [1, 2, *], Moshira M. Abd Elwahed [3, 4], Ahmed M. Ashour [2] and Shaimaa M. Faheem [5]

[1] Department of Pharmacology and Toxicology, Faculty of Pharmacy, Tobruk University, Libya.
[2] Chemistry department, Faculty of Science, Menoufia University, Egypt.
[3] Pathology department, Faculty of Medicine, Tobruk University, Libya.
[4] Pathology department, Faculty of Medicine, Menoufia University, Egypt.
[5] Medical laboratories department, High Technology Institute of Applied Health Sciences, Badr Academy, Badr City, Egypt.
* Corresponding Author

ORCID Details
Ahmed M. Ashour: https://orcid.org/0000-0002-7681-8306
Shaimaa M. Faheem: https://orcid.org/0009-0003-8820-1260

International Journal of Science and Research Archive, 2026, 20(02), 548–567

Publication history: Received on 12 July 2026; revised on 22 August 2026; accepted on 24 August 2026

Article DOI: https://doi.org/10.30574/ijsra.2026.20.2.1644



## ABSTRACT

Novel Fe(III), Mn(II), Co(II), Ni(II), Cu(II), Cd(II), Mg(II), Al(III), Zn(II), and Ba(II) complexes of an amido-salicylaldehyde ligand were synthesized and characterized by various analytical and spectroscopic techniques. The ligand coordinated as a neutral or dibasic pentadentate donor through imino nitrogen, hydroxyl oxygen, and amide oxygen atoms, forming distorted octahedral complexes. Conductivity measurements indicated non-electrolytic behavior. ESR studies revealed axial Cu(II) spectra with a dx2−y2 ground state, while Fe(III), Co(II), and Mn(II) complexes showed isotropic signals. Cytotoxicity studies against MCF-7 cells demonstrated enhanced activity after complexation, with the Zn(II) complex showing the highest potency compared with vinblastine sulfate. Molecular docking further supported the experimental cytotoxicity results through favorable binding interactions.

**Keywords:** Amido-Salicyldaldehyde, Complexes, Spectra, ESR, Magnetism, Conductivity, Cytotoxicity, Molecular Docking.

## 1 INTRODUCTION

Following the breakthrough discovery and clinical application of cisplatin as a mainstay chemotherapeutic agent, extensive research has been directed toward the development of non-platinum-based metallo drugs utilizing transition metals such as gold, ruthenium, copper, and zinc to overcome the severe systemic toxicities, off-target side effects, and

intrinsic or acquired resistance associated with platinum therapies [1]. These coordination compounds exert potent antitumor effects through diverse mechanisms, including modulating cellular metal ion homeostasis, depleting intracellular trace elements, and perturbing key signaling pathways governing malignant cell proliferation [2]. In this context, hydrazone ligands and their coordination complexes have emerged as highly versatile scaffolds in medicinal chemistry due to their facile synthesis, superior hydrolytic stability compared to conventional imines, and rich coordination chemistry provided by polydentate N,O-donor atom sets [3-5]. Moreover, complexation with transition metals significantly amplifies the intrinsic biological efficacy of parent hydrazone moieties [6]. Given that breast cancer (BC) remains the second most prevalent neoplasm globally and the leading cause of cancer-related mortality among women exhibiting distinct epidemiological profiles with lower median ages at diagnosis across Arab and African demographics, including Egypt there is an urgent imperative for novel targeted therapeutics [7-9]. Addressing this need, the present study details the design, synthesis, and comprehensive spectroscopic characterization of a novel series of transition metal complexes derived from an alanine-based hydrazone ligand. Furthermore, the cytotoxic potential of these synthesized complexes was rigorously evaluated against human breast adenocarcinoma (MCF−7) cell lines, complemented by in silico molecular docking simulations to elucidate their binding interactions and plausible mechanisms of action within key biological targets.

## 2 Experimental

### 2.1 Ligand synthesis

The ligand (**HL**) was synthesized through a three-step procedure. First, α-alanine was esterified in ethanol using concentrated $H_2SO_4$ under reflux for 3 h. The resulting α-alanine ester was then reacted with hydrazine under reflux at **70 °C for 3 h** to form the corresponding hydrazide. Finally, the product was reacted with salicylaldehyde in ethanol under reflux at **70 °C for 2–3 h.** After cooling, the precipitated product was filtered and dried to obtain the desired **HL ligand**.

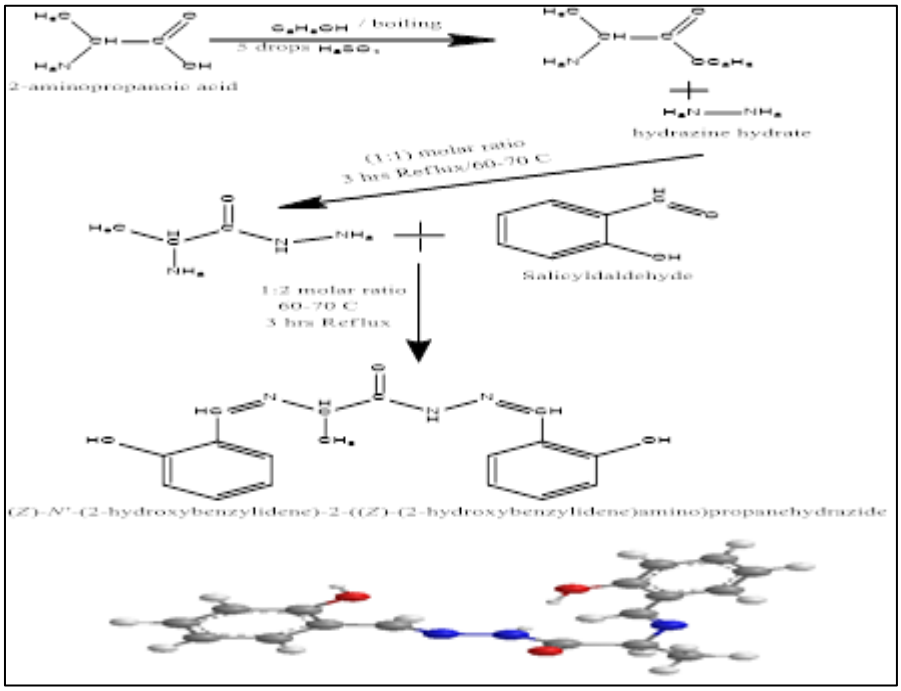


**Figure 1: Chemical and 3D Structures of the prepared [$H_3L$] Ligand.**

### 2.2 Metal complex preparation (2-20)

Metal complexes (**2–20**) were synthesized using a **1L:2M molar ratio** by refluxing the ligand with the corresponding metal salts in ethanol for **2 h at 80 °C** under continuous stirring. The resulting precipitates were filtered, washed, and dried over **$CaCl_2$** to obtain the desired metal complexes. For the **$BaSO_4$ complex (11),** five drops of HCl were added during the reaction. The synthesized complexes are presented in **Figure 2.2.3.**

### 2.3 Instruments and measurements

The synthesized compounds were characterized by **elemental analysis, TLC, FT-IR, $^{1}$H-NMR, MS, UV-Vis, TGA/DTA, molar conductivity, magnetic susceptibility, and ESR spectroscopy**. FT-IR and $^{1}$H-NMR analyses were performed using **JASCO FT/IR-300E** and **Bruker 350 MHz** instruments, respectively, while thermal behavior was evaluated using a **Shimadzu DT-30** analyzer. Magnetic properties and molar conductivity were measured by standard methods, and solid-state ESR spectra were recorded using a **Varian E-109 spectrometer with DPPH** as the reference.

### 2.4 Characterization via transmission electron microscopy (TEM)

Transmission electron microscopy (TEM) was employed to determine the **morphology, particle size, and distribution** of the ligand and its metal complexes. Colloidal suspensions were prepared in distilled water and deposited onto carbon-coated TEM grids, followed by air drying. The samples were then examined using a **JEOL 1230 TEM operated at 120 kV.**

### 2.5 Biological studies

#### 2.5.1 In vitro study

The **in vitro cytotoxicity** of the synthesized compounds was assessed using the **Sulforhodamine B (SRB) assay**. Cancer cells were seeded in 96-well plates, treated with different concentrations of the compounds in triplicate, and incubated for **48 h at 37 °C under 5% $CO_2$.** Cells were then fixed, stained with SRB, and the bound dye was dissolved in Tris-EDTA buffer. Absorbance was measured using an **ELISA reader**, and the survival fraction was calculated to determine the cytotoxic activity of the tested compounds

### 2.6 Study of toxicity

#### 2.6.1 Animals

Forty male Wistar albino rats (170–200 g) were obtained from the **National Cancer Institute (NCI-Egypt)** and housed under controlled conditions at **23–26 °C,** with adequate ventilation and a **10 h light/14 h dark** photoperiod. The animals were provided with a standard laboratory diet containing **12% bran, 50% ground corn meal, 12% corn oil, 19% ground beans, 4% casein, 2% minerals, and 1% vitamins**, along with purified water ad libitum. The diet was supplied by **Meladco Feed, Cairo, Egypt.**

#### 2.6.2 Acute toxicity

**Sixteen animals were used to determine the $LD_{50}$ values of the tested compounds. The $LD_{50}$ was evaluated to establish the** relationship between the administered dose and mortality, providing an indicator of the compounds' acute toxicity and potency. The determination was performed according to the method described by **Akhila et al. [12].**

#### 2.6.3 Experimental design

Twenty-four male Wistar albino rats (185 ± 15 g) were allowed to acclimatize and then randomly divided into three groups (n = 8). **Group I** served as the healthy control, **Group II** received the Cu(II) complex at a dose of $1 \times 10^{-5}$ mmol/L for 6 weeks, and **Group III** received the Zn(II) complex at the same dose for 6 weeks.

#### 2.6.4 Blood collection samples

Following the experimental period, all animals were fasted overnight and euthanized under light ether anesthesia. Blood samples were collected from the inferior vena cava and centrifuged at **4,000 rpm for 5–10 min**. The obtained serum/plasma and **EDTA-anticoagulated whole blood** were collected for subsequent **hematological and biochemical analyses.**

#### 2.6.5 Biochemical analyses:

Liver enzymes, Aspartate Aminotransferase (AST) and Alanine Aminotransferase (ALT) were measured via laboratory kits purchased from Human Diagnostic Kinetic Kits, Germany [13]. Serum albumin, blood urea, and serum creatinine levels were quantitatively determined using commercial diagnostic kits obtained from Diamond Diagnostics, Egypt, following the manufacturer's operational protocols [14].

#### 2.6.6 Hematological analyses:

The complete blood count (CBC) containing Hb% hemoglobin was measured via Drabkin's solution (prepared), and white blood cells (WBCs) or total leucocyte (TLC) counts, red blood cells (RBCs), and platelets (PLTs) counts were measured manually **[**15].

### 2.7 Statistical analysis

Statistical analysis was performed using one-way ANOVA, followed by Duncan's multiple range test as a post hoc analysis. Data were analyzed using SPSS version 20.0 and expressed as mean ± SD. Differences were considered statistically significant at $P \leq 0.05$ [16].

## 3 RESULTS AND DISCUSSION:

### 3.1 Physical properties

For a long time (a year), the ligand and its metal complexes were crystalline, nonhydrophilic, and pigmented when exposed in air at room temperature (R.T 25 $^{o}$C). These substances were insoluble in ethanol, water, benzene, methanol, and acetonitrile but soluble in dimethylsulfoxide (DMSO), dimethylformamide (DMF), nitromethane, nitrobenzene, and acetonitrile, chloroform and toluene. The chemical and physical analytical data shown in Table (1). Many effort have been made to prepare single or more crystals but unluckily. These efforts had failed. All acquired data fixed that, the formed (1 L: 2 M) molar ratio for all complexes.

**Table 1: Ligand [HL] and its Metal Complexes, Physical Data and Analytical Data.**

| No | Ligand/Complexes | Color | FW | M.P ($^{o}$C) | Yield (%) | Analysis /Found (Calculated.) (%) | | | |
|---|---|---|---|---|---|---|---|---|---|
| | | | | | | C | H | N | M |
| (1) | [$H_3L$] $C_{17}H_{17}N_3O_3$ | Greenish blue | 311 | 350 | 84 | 65.68 (64.90) | 5.50 (5.30) | 13.50 (13.45) | _ |
| (2) | [$(H_3L)(Cu)_2(CH_3COO)_4(H_2O)_2$].$2H_2O$ $C_{25}H_{33}N_3O_{14}Cu_2$ | green | 809 | >300 | 81 | 41.1 (40.9) | 5.8 (5.21) | 5.78 (5.55) | 17.49 (17.10) |
| (3) | [$(H_3L)(Mn)_2(CH_3COO)_4(H_2O)_2$]. $2H_2O$ $C_{25}H_{37}N_3O_{14}Mn_2$ | Off white | 739 | >300 | 85 | 42.13 (41.8) | 5.18 (4.8) | 5.92 (5.10) | 15.49 (14.10) |
| (4) | [$(H_3L)(Ni)_2(CH_3COO)_4(H_2O)_2$]. $2H_2O$ $C_{25}H_{37}N_3O_{14}Ni_2$ | greenish | 751 | >300 | 84 | 41.18 (41.00) | 5.89 (4.25) | 9.46 (9.50) | 14.37 (14.30) |
| (5) | [$(H_3L)(Zn)_2(CH_3COO)_4(H_2O)_2$].$2H_2O$ $C_{25}H_{34}N_3O_{14}Zn_2$ | Pale yellow | 756 | >300 | 78 | 41.12 (40.12) | 4.55 (4.30) | 9.75 (9.54) | 15.9 (15.12) |
| (6) | [$(H_3L)(Mg)_2(CH_3COO)_4(H_2O)_2$].$2H_2O$ $C_{25}H_{35}N_3O_{14}Mg_2$ | Orange | 709 | >300 | 79 | 45. 33 (45.23) | 5.13 (4.52) | 9.48 (9.85) | 7.50 (6.14) |
| (7) | [$(H_3L)(Co)_2(CH_3COO)_4(H_2O)_2$]. $2H_2O$ $C_{25}H_{34}N_3O_{14}Co_2$ | Reddish | 744 | >300 | 84 | 40.22 (40.12) | 4.09 (4.15) | 8.58 (8.65) | 22.81 (23) |
| (8) | [$(H_3L)(Cu)_2$ $(SO_4)_2$ $(H_2O)_4$]. $2H_2O$ $C_{17}H_{26}N_3O_{16}S_2Cu_2$ | Pale Blue Greenish | 746 | >300 | 79 | 28.41 (28.13) | 3.51 (3.0) | 8.85 (8.16) | 13.69 (13.52) |
| (9) | [$(H_3L)(Ni)_2$ $(SO_4)_2$ $(H_2O)_4$]. $2H_2O$ $C_{17}H_{31}N_3O_{18}S_2Ni_2$ | Dark Green | 775 | >300 | 82 | 27.3 (27.12) | 4.15 (4.12) | 5.6 (5.23) | 15.8 (15.3) |
| (10) | [$(H3L)(Co)_2(SO_4)_2(H_2O)_4$]. $2H_2O$ $C_{17}H_{25}N_3O_{16}S_2Co_2$ | Orange | 742 | >300 | 84 | 25.78 (25.32) | 3.55 (2.95) | 5.68 (5.23) | 11.62 (11.12) |
| (11) | [$(H_3L)(Ba)_2$ $(SO_4)_2$ $(H_2O)_4$]. $2H_2O$ $C_{17}H_{25}N_3O_{16}S_2Ba_2$ | Dark yellowish | 851 | >300 | 81 | 23.72 (24.01) | 3.13 (3.54) | 4.84 (4.96) | 31.64 (32.15) |
| (12) | [$(H_2L)(Fe)_2(SO_4)_2(H_2O)_4$]. $4H_2O$ $C_{17}H_{25}N_3O_{16}S_2Fe_2$ | Green | 767 | >300 | 77 | 26.75 (26.23) | 4.1 (3.95) | 5.54 (5.4) | 14.8 (14.3) |
| (13) | [$(H_3L)(Mg)_2$ $(SO_4)_2$ $(H_2O)_4$]. $2H_2O$ $C_{17}H_{25}N_3O_{16}S_2Mg_2$ | Dark yellow | 675 | >300 | 82 | 29.57 (30.12) | 2.91 (2.95) | 8.85 (8.45) | 31.71 (31.62) |
| (14) | [$(H_2L)(Al)_2(SO_4)_2(H_2O)_4$]. $2H_2O$ $C_{17}H_{25}N_3O_{16}S_2Al_2$ | Grayish | 679 | >300 | 75 | 31.53 (31.86) | 4.20 (4.56) | 6.49 (6.89) | 8.33 (8.56) |

| | | | | | | | | | |
|---|---|---|---|---|---|---|---|---|---|
| (15) | $[(H_3L)(Zn)_2\ (SO_4)_2\ (H_2O)_4].\ 4H_2O$ $C_{17}H_{25}N_3O_{16}S_2Zn_2$ | Pale green bluish | 783 | >300 | 81 | 28.19 (28.45) | 3.76 (4.02) | 5.80 (6.23) | 18.05 (18.54) |
| (16) | $[(H_3L)(Ni)_2(NO_3)_4(H_2O)_3].\ 3H_2O$ $C_{17}H_{21}N_7O_{18}Ni_2$ | Greenish | 777 | >300 | 85 | 27.51 (27.01) | 2.8 (2.9) | 13.2 (13.7) | 20.61 (20.01) |
| (17) | $[(H_2L)(Fe)_2\ (NO_3)_4\ (H_2O)_3].3H_2O$ $C_{17}H_{21}N_7O_{18}Fe_2$ | Light bluish | 769 | >300 | 84 | 28.24 (28.12) | 2.93 (2.85) | 7.56 (7.95) | 18.45 (19.01) |
| (18) | $[(H_3L)(Cd)_2\ (NO_3)_4\ (H_2O)_3].3H_2O$ $C_{17}H_{27}N_7O_{18}Cd_2$ | Offwhite | 863 | >300 | 76 | 23.8 (23.32) | 3.1 (2.85) | 11.4 (11.05) | 26.11 (25.82) |
| (19) | $[(H_3L)(Mg)_2(CO_3)_2(H_2O)_4].2H_2O$ $C_{19}H_{26}N_3O_{14}Mg_2$ | Brownish | 604 | >300 | 81 | 40.03 (39.54) | 4.77 (4.52) | 7.37 (7.12) | 8.53 (8.65) |
| (20) | $[(H_3L)(Cu)_2(CO_3)_2(H_2O)_4].4H_2O$ $C_{19}H_{34}N_3O_{18}Cu_2$ | Greenish | 780 | >300 | 84 | 28.5 (28.3) | 4.25 (4.13) | 5.25 (5.23) | 15.88 (15.37) |

### 3.2 IR spectra of the ligand [$H_3L$] (1) and its metal complexes

The FT-IR spectral analysis of the free ligand and its metal complexes (Table 2, Figures 2 and 3) elucidated the coordination mode and structural features. The spectrum of the free ligand displayed characteristic bands at 3450, 3373, 3190, 1700, and 1650 $cm^{-1}$, assigned to ν(OH), ν(N–H), ν(C=N), and ν(C=O) stretching vibrations, respectively, along with broad bands (3600–2670 cm−1) indicating intra- and intermolecular hydrogen bonding . Upon complexation, the shift of ν(C=N) and ν(C=O) to lower frequency regions (1675–1570 $cm^{-1}$ and 1682–1610 $cm^{-1}$) confirmed the coordination via azomethine nitrogen and carbonyl oxygen atoms, further evidenced by the emergence of new non-ligand bands at 610–640 $cm^{-1}$ (νM–N) and 520–580 $cm^{-1}$ (νM–O). Additionally, broad absorption in the 3570–3100 $cm^{-1}$ region confirmed the presence of hydrated or coordinated water, while characteristic bands at ~1220, 800, and 360 $cm^{-1}$ was attributed to inorganic anions ($NO_3^-$/$CO_3^{2-}$), alongside the ν(S=O) vibration of coordinated DMSO at ~1030 $cm^{-1}$ [17].

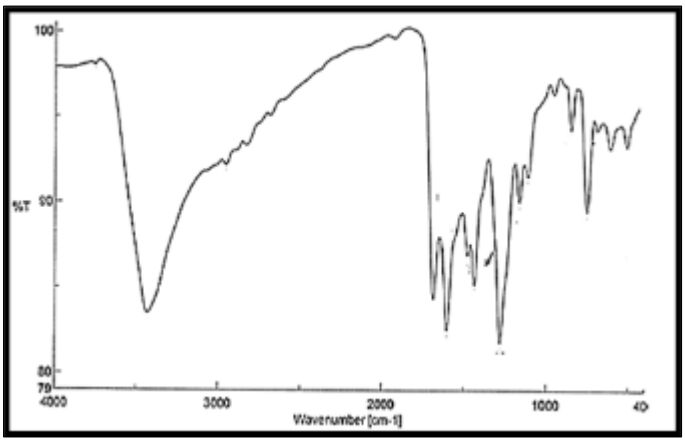


**Figure 2: IR spectrum of the Ligand**

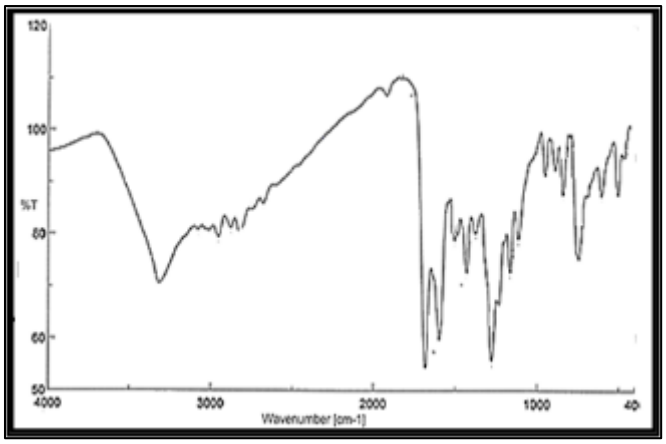


**Figure 3: IR spectrum of the Cu(II) complex**

**Table 2: IR Frequencies Bands ($cm^{-1}$) of the Ligand and its Metal Complexes.**

| No. | ν($H_2O$) | ν(OH) | υ(H-bondings) | ν(NH) | ν(C=O) | ν(C=N) | ν(Ar) | ν(OAc)/$SO_4$ | υ(M-O) | υ(M-N) |
|---|---|---|---|---|---|---|---|---|---|---|
| (1) | 3370-3220 | 3450,3373 | 3600-3320, 3380-2670 | 3190 | 1700 | 1650 | 1540,1450,818,750 | - | - | - |
| (2) | 3540-3250 | 3413,3365 | 3620-3320, 3210-2774 | 3175 | 1675 | 1610 | 1510,1435, 850.770 | 1240,1160 1110,750 | 610 | 580 |
| (3) | 3570-3280 3350-3225 | 3420,3372 | 3610-3320, 3319-2830 | 3160 | 1680 | 1615 | 1510,1435,850.770 | 1285,1180 1080,750 | 640 | 577 |
| (4) | 3560-3385 3310-3185 | 3410, 3320 | 3610-3190, 3180-2680 | 3180 | 1610 | 1616 | 1470,1438, 852,753 | 1252,1165 1082,755 | 635 | 583 |
| (5) | 3560-3370 3320-3180 | 3420,3379 | 3600-3210 3200-2700 | 3150 | 1610 | 1635 | 1486,1430, 850,765 | 1260,1125 1190,735 | 610 | 516 |
| (6) | 3340-3160 | 3415,3380 | 3560-3210 3200-2720 | 3170 | 1651 | 1610 | 1540,1515, 850,768 | 1230,1075 1110,770 | 615 | 513 |
| (7) | 3350-3185 | 3400, 3385 | 3645-3260 3210-3260 | 3187 | 1680 | 1605 | 1470,1438, 852,753 | 1260,1260 1093,690 | 640 | 520 |
| (8) | 3370-3130 | 3420, 3375 | 3650-3280, 3270-2650 | 3155 | 1615 | 1610 | 1486,1430,850,765 | 1430,1340 | 615 | 525 |
| (9) | 3510-3350 3315,3170 | 3418, 3245 | 3610-3330, 3310-2870 | 3180 | 1614 | 1612 | 1470,1438, 852,753 | 1354,1461 | 610 | 530 |
| (10) | 3325,3100 | 3422, | 3650-3330, 3320-2675 | 3178 | 1610 | 1615 | 1540,1515,850, 768 | 1465,1340 | 630 | 537 |

| | | | | | | | | | | |
|---|---|---|---|---|---|---|---|---|---|---|
| (11) | 3300,3150 | 3415 | 3640-3325, 3320-2870 | 3160 | 1682 | 1650 | 1486,1430,850,765 | 1480,1360 | 610 | 520 |
| (12) | 3320-3165 | 3420 | 3650-3350, 3340-2670 | 3170 | 1655 | 1670 | 1540,1515, 850,768 | 1470,1355 | 618 | 560 |
| (13) | 3325-3160 | 3415 | 3550-3340, 3340-2650 | 3150 | 1681 | 1664 | 1540,1510, 850,768 | 1430,1360 | 618 | 580 |
| (14) | 3365-3260 | 3432 ,3380 | 3610-3340, 3340-2675 | 3170 | 1676 | 1660 | 1540,1510, 850,768 | 1420,1210 | 615 | 515 |
| (15) | 3325-3160 | 3418 | 3650-3340, 3340-2610 | 3160 | 1670 | 1676 | 1540,1510, 850,768 | 1430,1240 | 610 | 510 |
| (16) | 3325-3180 | 3425 | 3620-3340, 3340-2610 | 3180 | 1650 | 1665 | 1540,1510, 850,768 | - | 618 | 520 |
| (17) | 3300-3170 | 3320 ,3300 | 3600-3320 3300-2700 | 3142 | 1670 | 1580 | 1550, 760 | - | 610 | 510 |
| (18) | 3340-3180 | 3410 3100 | 3540-3320 3310-2800 | 3150 | 1640 | 1570 | 1560, 754 | - | 615 | 580 |
| (19) | 3300-3170 | 3450 3110 | 3570-3340, 3300-2900 | 3150 | 1670 | 1610 | 1560, 850 | - | 618 | 570 |
| (20) | 3320-3180 | 3400 3100 | 3550-3300 | 3155 | 1675 | 1610 | 1555,765 | - | 618 | 520 |

### 3.3 $^{1}$H–NMR spectra

The **$^{1}$H-NMR spectra** of the ligand and its diamagnetic Zn(II) and Mg(II) complexes in DMSO-$d_6$ confirmed the proposed structures. The free ligand showed characteristic signals for **–$CH_3$, –CH=, and hydrazide –NH–N=C–** protons at 2.0/3.7, 5.4, and 8.9 ppm, respectively, with aromatic protons at 6.5–8.3 ppm. Upon complexation, the **–NH– and –CH=** signals shifted upfield to 8.0–8.3 and 4.8–5.1 ppm, respectively, confirming coordination of the **azomethine nitrogen to the metal center (M←N).**

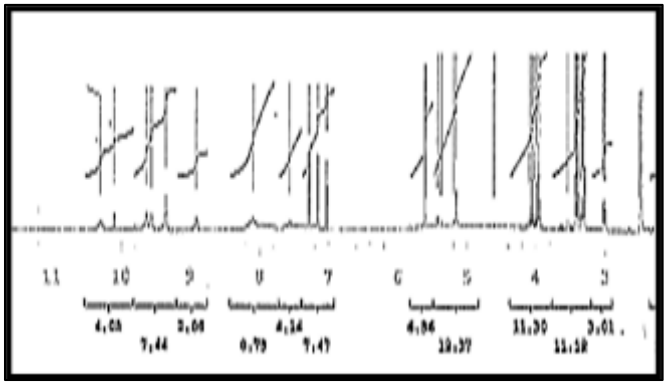

**Figure 4: $^{1}$H-NMR of the ligand**

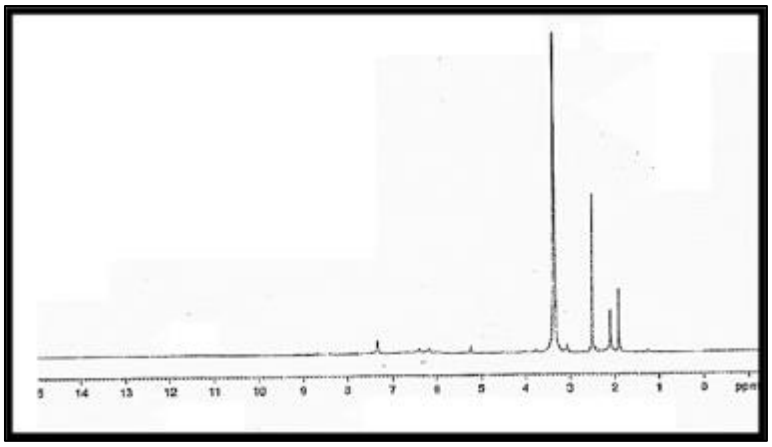

**Figure 5: 1H-NMR of the ZN(II) complex**

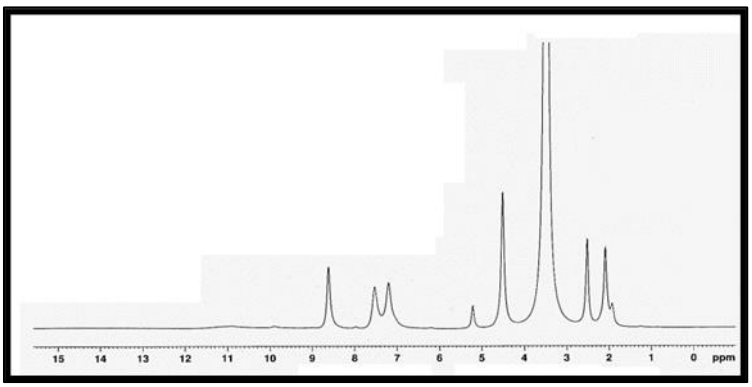


**Figure 6: $^{1}$H-NMR of the Mg$^{II}$ complex**

### 3.4 Conductance measurements

Molar conductance in various solvents of seven metal complexes ($1x10^{-3}$) was carried out to show the effect of solvent. The complexes displayed low molar conductivities as shown in table **(3).** Together the ligand and its metal complexes had non-electrolytic properties [18]. As shown as in figures 7 - 10 respectively.

**Table 3: Molar conductance in various solvents**

| Complex No | DMSO | DMF | Acetonitrile | Nitrobenzene | Acetone | Nitromethan |
|---|---|---|---|---|---|---|
| Complex (2) | 18 | 9.3 | 50 | 11 | 10 | 23 |
| Complex (3) | 20 | 10.7 | 57 | 14 | 12 | 24 |
| Complex (4) | 17 | 11.5 | 53 | 12 | 9.8 | 22 |
| Complex (5) | 15.8 | 8.7 | 48 | 11.7 | 9.5 | 20 |
| Complex (6) | 16 | 8 | 46 | 10.2 | 8.5 | 19 |
| Complex (7) | 16.8 | 10.2 | 54 | 12 | 10 | 22 |
| Complex (8) | 21 | 17 | 62 | 16 | 7.8 | 27 |

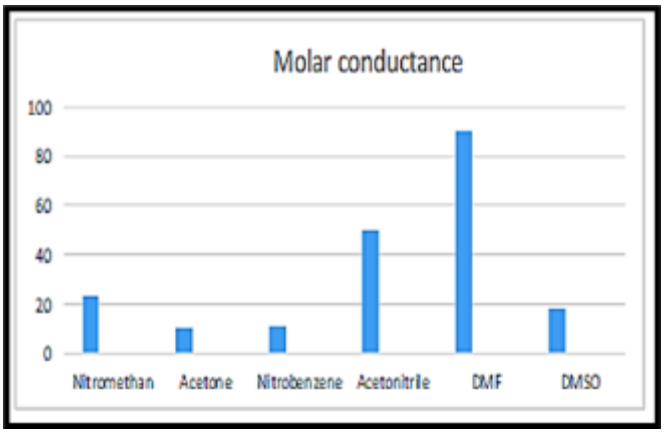


**Figure 7: Molar conductance for complex (2)**

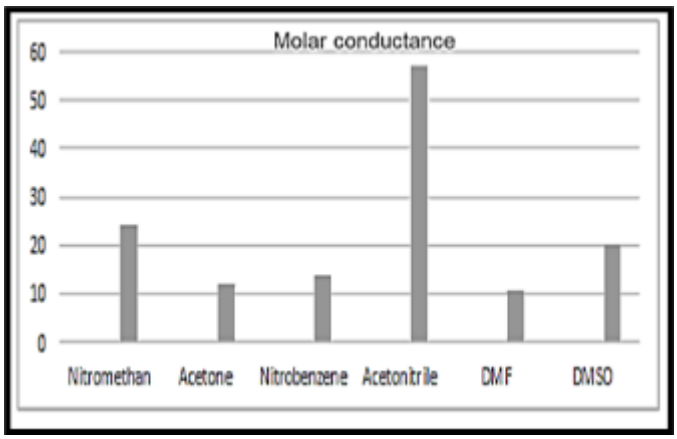


**Figure 8: Molar conductance for complex (3)**

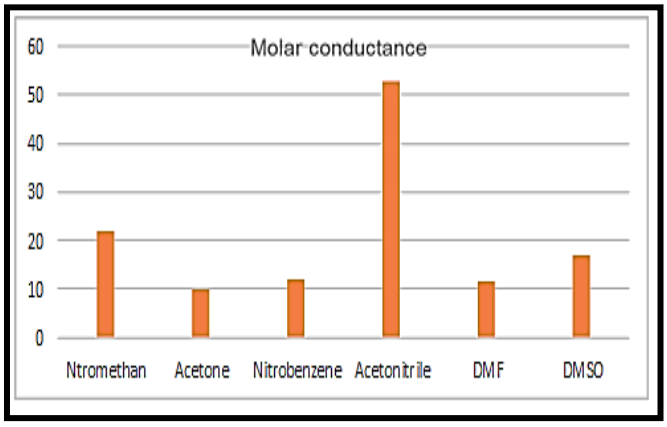


**Figure 9: Molar conductance for complex (4)**

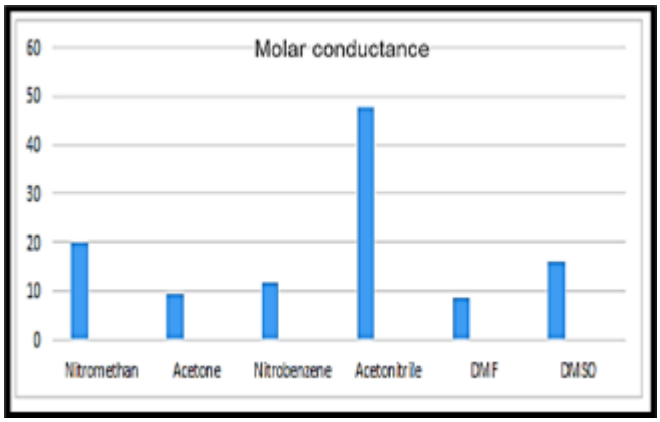


**Figure 10: Molar conductance for complex (5)**

### 3.5 Mass spectra

The mass spectrum of the ligand showed a molecular ion peak at *m/z* = 322, consistent with its calculated molecular mass and supporting the proposed structure. The characteristic fragment peaks at *m/z* = 54, 63, 90, 119, 221, 238, and 309 further confirmed the ligand framework. Similarly, the Zn(II) complex (5) exhibited a molecular ion peak at *m/z* = 728, in agreement with its calculated molecular mass. The characteristic fragmentation peaks at *m/z* = 54.89, 219, 238, 509, and 548 provided additional support for the proposed structure. The mass spectra of the ligand and Zn(II) complex (5) are shown in Figures 11 and 12, respectively.

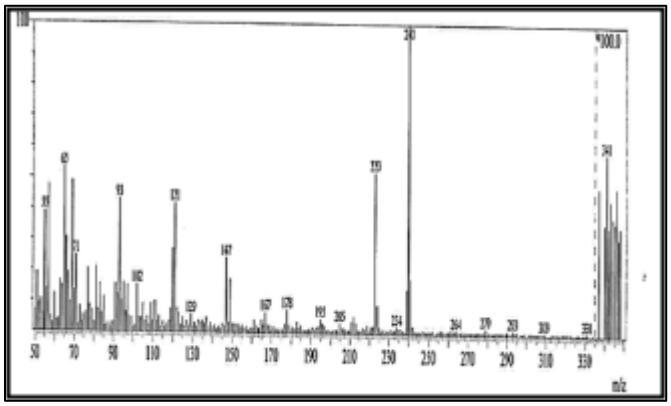

**Figure 11: Mass spectrum of the ligand**

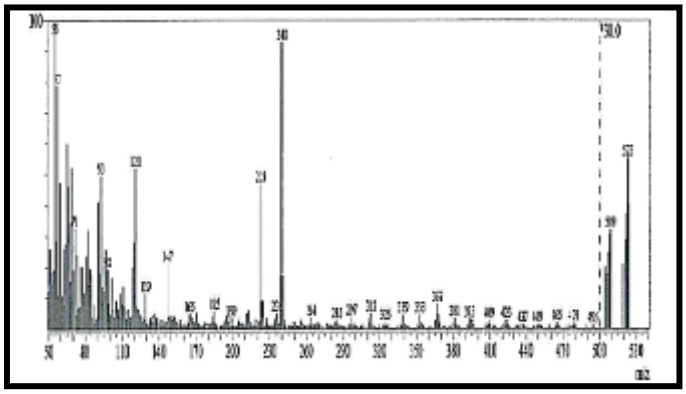

**Figure 12: Mass spectrum of the ZN(II)**

### 3.6 Electronic spectra

The electronic absorption spectrum of free [HL] exhibited three characteristic bands at 280, 310, and 350 nm (π→ π*, n→ π*, and CT transitions), while its metal complexes displayed corresponding intraligand transitions alongside diagnostic d–d bands [20]. Specifically, Cu II complexes (**2, 8, 20**) exhibited d–d absorption in the 430–620 nm region with magnetic moments of 1.69–1.71 B.M., indicating a Jahn-Teller distorted octahedral geometry ($d^9$). NiII complexes (**4, 9, 16**) displayed d–d transitions at 440–745 nm with magnetic moments of 3.01–3.14 B.M., supporting a distorted octahedral environment (ν2/ν1=1.59–1.64). Furthermore, MnII, CoII (μeff=4.48–4.80 B.M.), and FeIII (μeff=5.80–6.12 B.M.) complexes revealed characteristic high-spin octahedral geometries, whereas the remaining diamagnetic complexes were dominated exclusively by intraligand transitions [21].

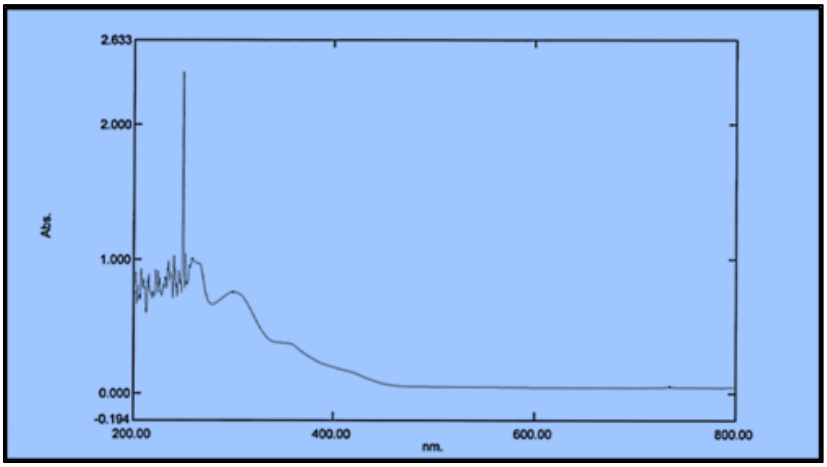


**Figure 13: Electronic spectrum of the Zn II**

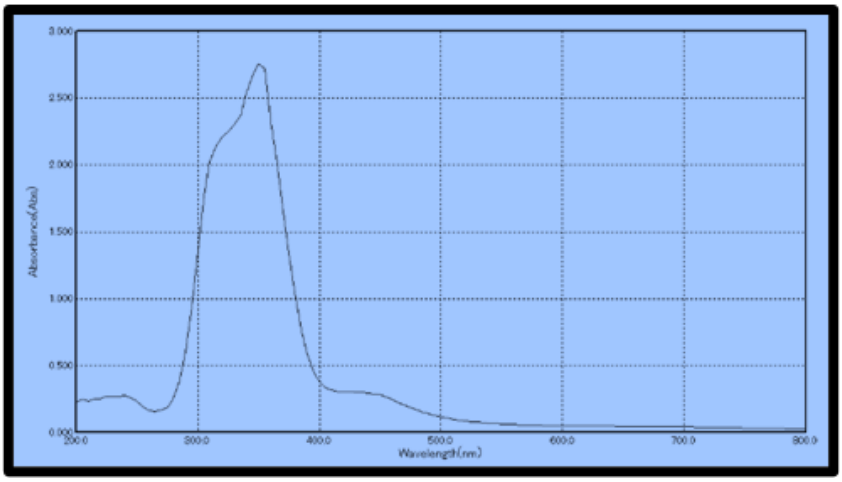


**Figure 14: Electronic spectrum of the Cu II**

**Table 4: B.M., the prepared compounds' magnetic moments, and electronic absorption spectral bands (nm).**

| Comp. No. | $\lambda_{max}$ (nm) | μeff. |
|---|---|---|
| (1) | 280, 310, 350 | - |
| (2) | 250, 310, 320, 450, 550, 620 | 1.71 |
| (3) | 260, 310, 410, 490, 580, 615 | 5.65 |
| (4) | 260, 310, 440, 560, 620, 720 | 3.01 |
| (5) | 250, 310, 300 | Diamagnetic |
| (6) | 250, 310, 320 | Diamagnetic |
| (7) | 260, 310, 380, 410, 580, 610 | 4.48 |

| | | |
|---|---|---|
| (8) | 260, 310, 450, 520, 610 | 1.69 |
| (9) | 275, 320, 410, 450, 530, 610,740 | 3.16 |
| (10) | 270, 310, 440, 570, 625 | 4.80 |
| (11) | 260, 320, 310 | Diamagnetic |
| (12) | 260, 310,460,520,620 | 5.80 |
| (13) | 250, 270, 310 | Diamagnetic |
| (14) | 260, 280, 310 | Diamagnetic |
| (15) | 260,300,310 | Diamagnetic |
| (16) | 260, 310, 460, 540, 600, 730 | 3.4 |
| (17) | 260, 310, 450, 560, 620 | 6.12 |
| (18) | 270, 310, 300 | Diamagnetic |
| (19) | 270, 310, 300 | Diamagnetic |
| (20) | 260,300, 310, 430, 560,615 | 1.71 |

### 3.7 Thermal analysis [22]

Thermal stability and decomposition pathways of representative complexes (2, 3, 12, 18, and 20) were investigated by TG/DTA under a nitrogen atmosphere (Table 5). The thermograms showed a multistep decomposition pattern. The initial endothermic event at 40–50°C was attributed to hydrogen-bond cleavage, followed by the loss of lattice water below 85°C. Further endothermic steps at 125–140°C and 160–250°C corresponded to the loss of coordinated water and coordinated anions, respectively. The experimental weight losses were in good agreement with the calculated values. Subsequent thermal decomposition at higher temperatures involved degradation of the organic ligand framework, ultimately leaving the corresponding metal oxides (CuO, MnO, NiO, FeO, or CdO) as stable residues. These results confirm the good thermal stability and proposed compositions of the investigated complexes.

**Table 5: Thermal analyses of some Metal complexes**

| **Compound No.** | **Temp. (°C)** | **DTA (peak)** | | **TGA (Wt.loss %)** | | **Assignments** |
|---|---|---|---|---|---|---|
| | | Endo | Exo | Calculated. | Found | |
| (2) | 45 | Yes | No | 0 | 0 | Broken of H-bondingss |
| | 70<br>125 | Yes<br>Yes | No<br>No | 2.46<br>7.58 | 2.30<br>7.45 | Loss of ($H_2O$) hydrated water<br>Loss of ($3H_2O$) molecules |
| | 160 | Yes | No | 25.40 | 23.9 | Loss of (2OAC) group |
| | 320 | No | Yes | 0 | 0 | Melting point |
| | 570 460,510,540, | No | Yes | 37.7 | 37.4 | Decomposition process with the formation of 2CuO |
| (3) | 50 | Yes | No | 0 | 0 | Broken of H-bondingss |
| | 85 | Yes | No | 2.52 | 2.41 | Loss of ($H_2O$) hydrated water molecule |
| | 135 | Yes | No | 7.8 | 7.65 | Loss of ($3H_2O$) Coordinated water |
| | 185 | Yes | No | 36.76 | 36.52 | Loss of 4(OAC) group |
| | 360 | No | Yes | 0 | 0 | Melting point |
| | 400,440,475,560,570 | No | Yes | 35.1 | 34.82 | Decomposition process with the formation of 2Mn |
| | 40 | Yes | No | 0 | 0 | Broken of H-bondingss |

| | | | | | | |
|---|---|---|---|---|---|---|
| (9) | 80 | Yes | No | 8.2 | 8.1 | Loss of ($2H_2O$) hydrated water molecules |
| | 140 | Yes | No | 12.69 | 12.13 | Loss of ($5H_2O$) Coordinated water molecules |
| | 250 | Yes | No | 31.02 | 30.92 | Loss of $2SO_4$ group |
| | 340 | No | Yes | 0 | 0 | Melting point |
| | 420,440,480, 550,580 | No | Yes | 35.13 | 35.0 | Decomposition process with the formation of 2NiO |
| (12) | 45 | Yes | No | 0 | 0 | Broken of H-bondingss |
| | 70<br>130 | Yes<br>Yes | No<br>No | 4.75<br>12.45 | 4.56<br>12.21 | Loss of ($2H_2O$) hydrated water molecules<br>Loss of ($5H_2O$) coordinated water molecule |
| | 240 | Yes | No | 30.38 | 30.12 | Loss of $2SO_4$ group |
| | 340 | No | Yes | 0 | 0 | Melting point |
| | 410,510,540,600 | No | Yes | 32.72 | 32.51 | Decomposition process with the formation of 2FeO |
| (18) | 45 | Yes | No | 0 | 0 | Broken of H-bondingss |
| | 75 | Yes | No | 4.2 | 3.95 | Loss of($2H_2O$) hydrated water molecules |
| | 140 | Yes | No | 6.6 | 6.52 | Loss of($3\ H_2O$)Coordinate water molecules |
| | 235 | Yes | No | 32.3 | 32.0 | Loss of($4NO_3$) |
| | 320 | No | Yes | 0 | 0 | Melting point |
| | 340,370,440,510,580 | No | Yes | 18.1 | 17.98 | Decomposition process with the formation of 2CdO |
| (20) | 40 | Yes | No | 0 | 0 | Broken of H-bondingss |
| | 70 | Yes | No | 5.75 | 5.54 | Loss of ($3H_2O$) hydrated water molecules |
| | 140 | Yes | No | 12.1 | 11.98 | Loss of ($5H_2O$) coordinated water molecules |
| | 210 | Yes | | 17.9 | `17.7 | Loss of ($2CO_3$) group |
| | 370 | No | Yes | 0 | 0 | Melting point |
| | 380,440,510,540,610 | No | Yes | 23.69 | 23.35 | Decomposition process with the formation of 2CuO |

### 3.8 Electron spin resonance (ESR):

The solid-state ESR spectra provided key insights into the coordination geometries and bonding characteristics of the metal complexes. The CuII complexes (2, 8, 20) exhibited axial spectra with $g_{\parallel}>g_{\perp}>2.0024$, confirming a $d_{x^2-y^2}$ (2B1g) ground state in a tetragonally distorted octahedral environment ($g_{\parallel}/A_{\parallel}$=153.4–179.0 cm). The exchange parameter ($G\geq4.0$) indicated negligible spin-exchange coupling between copper centers. Evaluated bonding parameters ($K<1.0$, $g_{\parallel}<2.31$, $\alpha^2$=0.60–0.71, and $\beta_1^2$=0.88–0.94) demonstrated significant in-plane σ- and π-covalency, whereas out-of-plane π-interaction ($\beta^2>1.0$) was predominantly ionic, aligned with calculated %$ad^2$ values (52.5–64.9%). In contrast, the MnII, CoII, and FeIII complexes displayed isotropic signals ($g_{iso}$=2.001–2.050), characteristic of distorted octahedral geometries [23].

**Table 6: Electron spin resonance data of some metal complexes**

| Complex | $g_{\parallel}$ | $g_{\perp}$ | $g_{iso}$[a] | $A_{\parallel}$ (G) | $A_{\perp}$ (G) | $A_{iso}$[b] (G) | G[c] | $\Delta E_{xy}$ ($cm^{-1}$) | $\Delta E_{xz}$ ($cm^{-1}$) | $K_{\perp}^2$ | $K_{\parallel}^2$ | $K^2$ | K | $g_{\parallel}/A_{\parallel}$ ($cm^{-1}$) | $\alpha^2$ | $\beta^2$ | $_1\beta^2$ | $-2\beta$ | $a^2d$ (%) |
|---|---|---|---|---|---|---|---|---|---|---|---|---|---|---|---|---|---|---|---|
| (2) | 2.241 | 2.062 | 2.12 | 140 | 5.0 | 50 | 4.0 | 17543 | 22831 | 0.79 | 0.63 | 0.74 | 0.87 | 153.4 | 0.71 | 1.1 | 0.89 | 152.5 | 64.9 |
| (3) | - | - | 2.007 | - | - | - | - | - | - | - | - | - | - | - | - | - | - | - | - |
| (8) | 2.20 | 2.051 | 2.10 | 120 | 7.5 | 45 | 4.0 | 17699 | 22472 | 0.65 | 0.53 | 0.61 | 0.78 | 179 | 0.6 | 1.08 | 0.88 | 123 | 52.5 |
| (11) | - | - | 2.0011 | - | - | - | - | - | - | - | - | - | - | - | - | - | - | - | - |
| (12) | - | - | 2.003 | - | - | - | - | - | - | - | - | - | - | - | - | - | - | - | - |
| (17) | - | - | 2.05 | - | - | - | - | - | - | - | - | - | - | - | - | - | - | - | - |
| (20) | 2.231 | 2.0551 | 2.112 | 125 | 5.0 | 45 | 4.18 | 17857 | 22989 | 0.73 | 0.61 | 0.69 | 0.83 | 171.5 | 0.65 | 1.12 | 0.94 | 133 | 56.7 |

Based on all the aforementioned studies, the proposed chemical structures of the investigated metal complexes are illustrated as follows

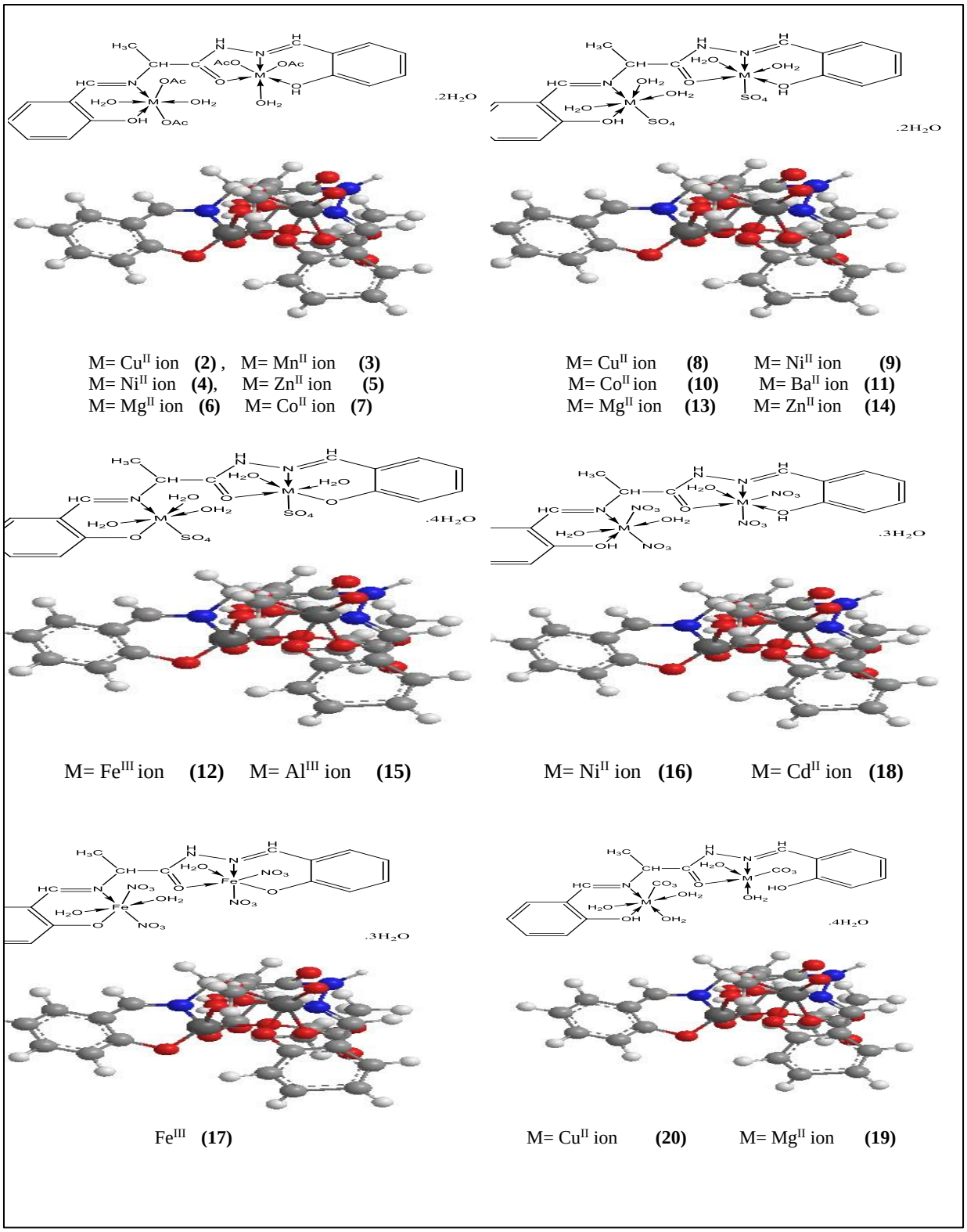


**Figure 15: Chemical and 3D structures of the prepared metal complexes.**

### 3.9 Transmission electron microscopy (TEM) characterization

Copper II complex**(2)** and Zinc II complex**(5)** complexes had average diameters of 21.875±6.989 nm and 12.11±1.336 nm, respectively. Each particle had a diameter of 1 to 100 nm and a size of a nanometer. These compounds were present as nanoparticles, as seen in Figures (3) and (4).

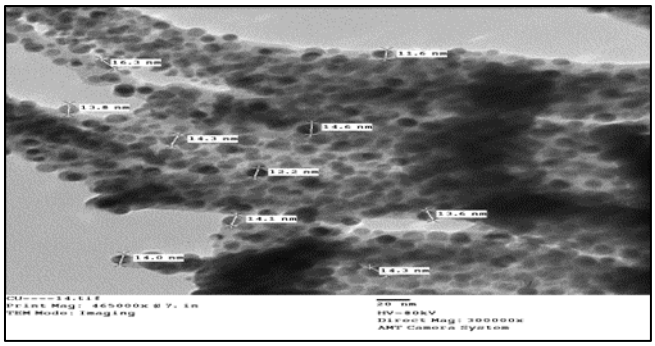

**Figure 16: Copper II complex nanoparticles**

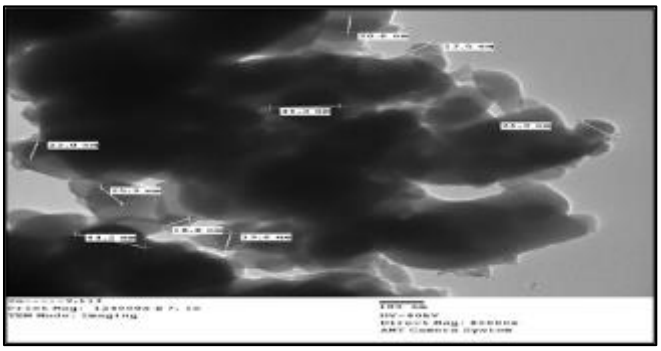

**Figure 17: Zinc II complex nanoparticles**

When compared to large-sized particles, metal complexes exhibited new or reinforcing size-dependent features for the material or compounds. The complex particles were created as nanosized particles, meaning their diameter ranged from 1 to 100 nm. They also offer numerous advantages and benefits, including a smaller dosage form, stable dosage forms, improved bioavailability, reduced toxicity, dose proportionality, and many more for a variety of medications. [24, 25].

### 3.10 In vitro cytotoxicity:

The cytotoxic activity of the ligand and its metal complexes (2), (5), and (7) was evaluated against human breast cancer (MCF-7) cells. All complexes showed greater anticancer activity than the free ligand, consistent with Tweedy's chelation theory. Among the tested compounds, Zn(II) complex (7) exhibited the highest potency, with an $IC_{50}$ of 5.01 μM, followed by complexes (2) and (5), with $IC_{50}$ values of 30.0 and 31.6 μM, respectively. The enhanced activity may be attributed to metal chelation, which modifies the electronic properties, lipophilicity, and DNA-binding ability of the complexes. The observed cytotoxicity may also involve ROS generation and oxidative stress, contributing to the dose-dependent reduction in MCF-7 cell viability [26].

#### 3.10.1 Overview of In Vivo Toxicity Assessments

As detailed in Table 10, liver function evaluation based on plasma albumin levels and key hepatic enzymes (ALT and AST) showed no statistically significant toxicological differences between the standard control group and the treated groups in normal rats. Furthermore, renal function markers (serum creatinine and blood urea nitrogen) as well as comprehensive hematological parameters (Table 11 and Table 12) exhibited no significant adverse variations following administration of Copper(II) and Zinc(II) complexes, confirming the biological safety profile of these coordination compounds at a dosage of $1\times10^{-3}$ mmol/L.

**Table 10: Statistical analysis (ANOVA) of liver function parameters among the experimental groups.**

| Enzymes / Parameters | Units | Group (I) Standard Control | Group (II) Copper(II) Complex | Group (III) Zinc(II) Complex |
|---|---|---|---|---|
| ALT (Alanine Aminotransferase) | U/L | 53.538 ± 4.508 | 32.789 ± 5.190 | 47.142 ± 3.874 |
| AST (Aspartate Aminotransferase) | U/L | 81.651 ± 7.911 | 56.726 ± 4.240 | 88.211 ± 5.810 |
| Albumin | g/dL | 5.150 ± 2.197 | 5.113 ± 2.760 | 4.091 ± 1.229 |

Note: Values are expressed as Mean ± Standard Deviation (SD). Statistical analysis was performed using one-way ANOVA ($p < 0.05$). Means sharing the same superscript letters within a row are not significantly different from each other. Treatments were administered at a concentration of $1\times10^{-5}$ mmol/L.

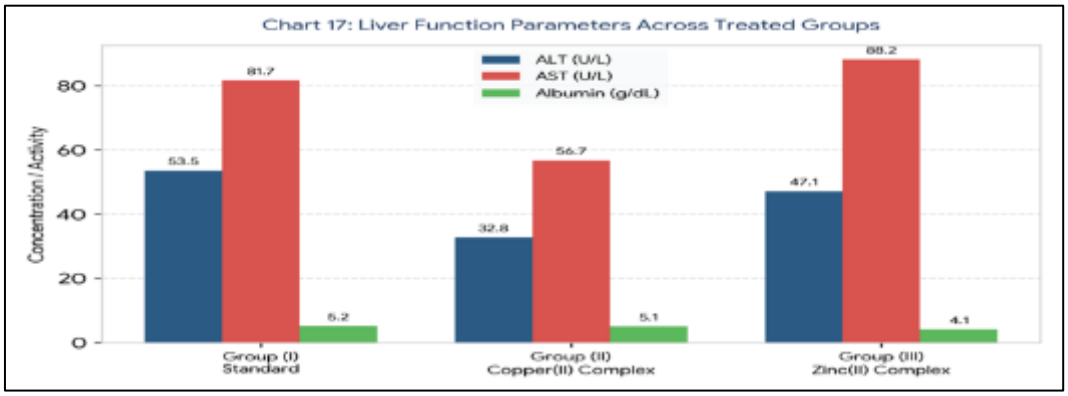


**Figure 18: Liver enzyme activities (ALT, AST) and albumin concentrations across experimental groups.**

**Table 11: Statistical analysis (ANOVA) of renal function tests among the experimental groups.**

| Kidney Parameters | Units | Group (I) Standard Control | Group (II) Copper(II) Complex | Group (III) Zinc(II) Complex |
|---|---|---|---|---|
| Blood Urea | mg/dL | 34.166 ± 3.594 | 31.819 ± 2.007 | 38.005 ± 3.101 |
| Serum Creatinine | mg/dL | 1.504 ± 0.199 | 1.499 ± 0.101 | 1.536 ± 0.100 |

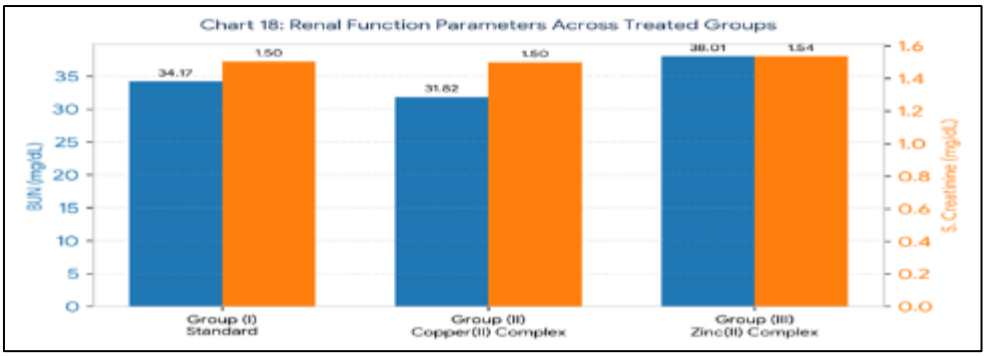


**Figure 19: Renal function parameters (B.Urea and Serum Creatinine) across experimental groups.**

**Table 12: Statistical evaluation (ANOVA) of hematological parameters across experimental groups.**

| Hematological Parameter (CBC) | Units | Group (I) Standard Control | Group (II) Copper(II) Complex | Group (III) Zinc(II) Complex |
|---|---|---|---|---|
| Hemoglobin (Hb) | g/dL | 14.966 ± 2.842 | 14.891 ± 2.012 | 15.003 ± 2.112 |
| Red Blood Cells (RBCs) | $\times 10^6$/cmm | 5.730 ± 0.591 | 5.997 ± 0.709 | 6.180 ± 0.819 |
| Total Leukocyte Count (TLC) | $\times 10^3$/cmm | 9.998 ± 0.983 | 8.896 ± 1.019 | 9.981 ± 0.783 |
| Platelets (PLTs) | $\times 10^3$/cmm | 528.269 ± 37.974 | 489.308 ± 21.891 | 519.892 ± 32.612 |

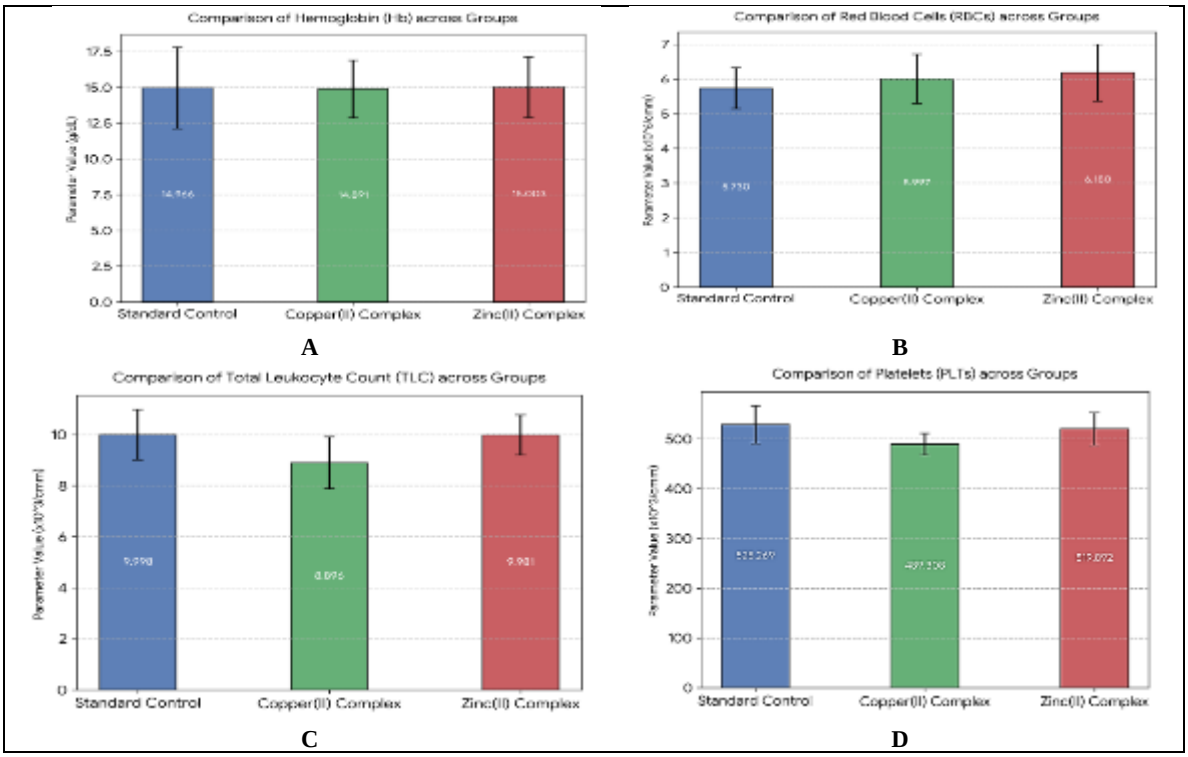


**Figure 20: A, B, C and D: Hematological parameters across experimental groups**

## 4 CONCLUSION

Nano-organometallic complexes of Fe(III), Mn(II), Co(II), Ni(II), Cu(II), Cd(II), Mg(II), Al(III), Zn(II), and Ba(II) with an amido-salicylaldehyde ligand were successfully synthesized and characterized using spectroscopic and thermal techniques. The complexes were predominantly octahedral and non-electrolytic, with considerable covalent character. Biological studies showed enhanced, dose-dependent cytotoxicity against MCF-7 breast cancer cells compared with the free ligand, in agreement with Tweedy's chelation theory [25]. Molecular docking further demonstrated favorable interactions with the target protein active sites, supporting the potential of these nano-organometallic complexes as promising anticancer candidates.

## STATEMENTS ON COMPLIANCE WITH ETHICAL STANDARDS

### *Acknowledgments*

The authors are profoundly grateful to the Department of Chemistry, Faculty of Science, Menoufia University, and the Department of Pharmacology and Toxicology, Faculty of Pharmacy, Tobruk University, as well as all individuals and institutions whose valuable support and resources made this research possible.

### *Funding Source*

This research received no specific grant from any funding agency in the public, commercial, or not for profit sectors.

### *Disclosure of conflict of interest*

The authors have declared no conflict of interest.

### *Statement of ethical approval*

This study was performed after getting permission from the Institutional Animal Ethical Committee, Menoufia University, Egypt (approval ID: MUFS/S/CH/1/25).

### *Statement of informed consent*

This study did not involve human participants, and therefore, informed consent was not required.

### *Author's Contributions*

A. S. El-Tabl and M.M. Abd Elwahed designed the study and performed the complexes synthesis. A. M. Ashour, R. M. Mustafa and M. F. Mohamed performed most of the experiments. A. M. Ashour and S.M. Faheem analyzed and interpreted the data. A. S. El-Tabl and A.M. Ashour wrote the first version of the manuscript. All authors reviewed and approved the final version of the manuscript.

## REFERENCES


[1] Zhang, C., Xu, C., Gao, X., & Yao, Q. (2022). Platinum-based drugs for cancer therapy and anti-tumor strategies. *Theranostics*, *12*(5), 2115.

[2] Kostova, I. (2026). Heterometallic Multinuclear Ruthenium Complexes as Cytotoxic Agents. *Biomedicines*, *14*(5), 1028.

[3] Wu, X., Geng, S., & Yang, J. (2026). Metabolism-Regulating Nanomedicines for Cancer Therapy. *Advanced NanoBiomed Research*, *6*(1), e202500105.

[4] Islam, R., Khatun, N., Islam, R., Islam, M. R., Alam, J., Rahaman, M. H., & Al Ayub, S. B. (2025). Clinicopathological Features of Liver Metastasis of Solid Tumors at National Institute of Cancer Research and Hospital. *Asia Pacific Journal of Medical Innovations*, *2*(2), 24.

[5] Wilkinson, L., & Gathani, T. (2022). Understanding breast cancer as a global health concern. *The British journal of radiology*, *95*(1130), 20211033.

[6] Elhawary, N. A., Ekram, S. N., Sembawa, H. A., Tashkandi, E., Bannani, S., Azher, Z. A & Elhawary, A. N. (2025). Descriptive epidemiology of female breast cancer around the world: incidence, mortality, and sociodemographic risks and disparities. *International Journal of Environmental Health Research*, *35*(12), 3648.

[7] ROHEEL, Amna, et al. Global epidemiology of breast cancer based on risk factors: a systematic review. *Frontiers in Oncology*, 2023, 13: 1240098.

[8] Liu, Y., Yang, X., He, Z., Li, J., Li, Y., Wu, Y.& Xiang, H. (2023). Spinal cord injury: global burden from 1990 to 2019 and projections up to 2030 using Bayesian age-period-cohort analysis. *Frontiers in neurology*, *14*, 1304153.

[9] Eden, C. M., Johnson, J., Syrnioti, G., Malik, M., & Ju, T. (2023). The Landmark Series: The Breast Cancer Burden of the Asian American Population and the Need for Disaggregated Data: CM Eden et al. *Annals of surgical oncology*, *30*(4), 2121-2127.

[10] El-Tabl, A. S., Dawood, A. A. E. R., Kolkaila, S., Mohamed, E. H., & Ashour, A. (2023). The Cytotoxicity of Some Biologically Active Nano Compounds against Colon Cancer: Advanced Biochemical Analyses. *TWIST*, *18*(4), 360.

[11] Shakil, M. S., Rana, Z., Hanif, M., & Rosengren, R. J. (2022). Key considerations when using the sulforhodamine B assay for screening novel anticancer agents. *Anti-cancer drugs*, *33*(1), 6.

[12] Akhila, J. S., Shyamjith, D., & Alwar, M. C. (2007). Acute toxicity studies and determination of median lethal dose. *Current science*, 917.

[13] Abdel-Rahman, O. N., Radwan, S. A., Abdelrahman, A. F., Mohammad, A. A., & Abdel-Baky, E. S.(2024) Study the Effect of Vitamin C against Methomyl Toxicity on Hematological and Biochemical Parameters in Male Albino Rats. *The Egyptian Journal of Hospital Medicine*, *97*, 4457.

[14] Elkhabery, S., Ashour, A. M., El Tabl, A. S., Abd El Wahed, M. M., Ismail, A. H. A., & Abu-Setta, M. H. (2026). A Multimodal Study on the Ameliorative Potential of Metallo-Organic Compounds against Hepatocellular Carcinoma: Biochemical, Histological, Immunohistochemical, and Molecular Docking Approaches. *Egyptian Journal of Chemistry*, *69*(7), 437.

[15] Ullah, A., Akhtar, J., & Khan, M. S. (2021). Correlation of blood Complete Performed by Hematology Analyzer with manual methods at District Bannu Khyber Pakhtunkhwa, Pakistan. *BMC Journal of Medical Sciences*, *2*(2), 24.

[16] Nainggolan, Y., Divia, D., Hutapea, D. L., Sirait, W. F., Sirait, M., & Sianturi, R. (2025). Anava Satu Jalur (One Way–Anova). *Innovative: Journal Of Social Science Research*, *5*(1), 5670.

[17] Pasieczna-Patkowska, S., Cichy, M., & Flieger, J. (2025). Application of Fourier transform infrared (FTIR) spectroscopy in characterization of green synthesized nanoparticles. *Molecules*, *30*(3), 684.

[18] Santanilla, A. J. M., Aliprandini, P., Benvenuti, J., Tenorio, J. A. S., & Espinosa, D. C. R. (2021). Structure investigation for nickel and cobalt complexes formed during solvent extraction with the extractants Cyanex 272, Versatic 10 and their mixtures. *Minerals Engineering*, *160*, 106691.

[19] Abd El-Nasser, M. G., & Ismail, T. I. (2025). Synthesis, characterization, molecular docking studies, and theoretical calculations of novel Ni (II), Cu (II), and Zn (II) complexes based on benzothiazole derivative. *BMC chemistry*, *19*(1), 202.

[20] Marchetti, F., Pettinari, R., Verdicchio, F., Tombesi, A., Scuri, S., Xhafa, S. & Galindo, A. (2022). Role of hydrazone substituents in determining the nuclearity and antibacterial activity of Zn (II) complexes with pyrazolone-based hydrazones. *Dalton Transactions*, *51*(37), 14165.

[21] Al-Daffay, R. K. H., & Al-Hamdani, A. A. S. (2023). Synthesis, characterization, and thermal analysis of a new acidicazo ligand's metal complexes. *Baghdad Science Journal*, *20*(1), 0121-0121.

[22] El-Desouky, M. G., El-Bindary, A. A., El-Afify, M. A. M., & Hassan, N. (2022). Synthesis, characterization, theoretical calculation, DNA binding, molecular docking, anticovid-19 and anticancer chelation studies of some transition metal complexes. *Inorganic and Nano-Metal Chemistry*, *52*(9), 1273-1288.

[23] Sellies, L., Spachtholz, R., Bleher, S., Eckrich, J., Scheuerer, P., & Repp, J. (2023). Single-molecule electron spin resonance by means of atomic force microscopy. *Nature*, *624*(7990), 64-68.

[24] El-Tabl, A. S., Abd El-Wahed, M. M., Ahmed, R. A. S., Alhalib, A. A. A., & Ashour, A. M. (2022). Physico-chemical Characterization and Estimation of Antimicrobial Activity of Modified Aspirin in the form of Nano-organometallic Compounds. *Chemical Science International Journal*, *31*(3), 11.

[25] Faheem, S. M., Osman, H. M., El-Tabl, A. S., Abd-El Wahed, M. M., & Younes, S. M. (2024). New nano-complexes targeting protein 3S7S in breast cancer and protein 4OO6 in liver cancer investigated in cell line. *Scientific Reports*, *14*(1), 16891.

[26] Li, W., Liu, S., Ding, H., Zhao, R., Zang, P., Li, S. & Yang, P. (2024). Three-step depletion strategy of glutathione: tunable metal–organic-framework-engineered nanozymes for driving oxidative/nitrative stress to maximize ferroptosis therapy. *Nano Letters*, *24*(6), 2071-2080.